Characterization of Aging Propagation in Lithium-ion Cells Based on an Electrochemical Model

Anirudh Allam, Simona Onori, *Senior Member, IEEE*

***Abstract*— In this paper, we use an electrochemical degradation model to characterize aging propagation in Lithium-ion (Li-ion) battery cells. The three-time scale behavior of individual cells is formally studied using a singular perturbation theory approach. The resulting reduced aging battery model is used to quantify the aggravated degradation occurring to each cell, within an interconnected configuration, due to existing cell-to-cell variation, in the form of an aging gradient. Simulation results show the context-dependent aging propagation in the case of four cells connected in series.**

I. Introduction

Battery packs are composed of individual battery cells (hundreds or thousands, [1], [2]) connected either in series and/or parallel. Neither of the individual cells are created equal, nor do they degrade equally upon usage. Production tolerances, uneven temperature distribution, and differences in the aging characteristics of cells, cause overstress in individual cells that are connected in series, resulting in premature failure. The decreased life cycle decreases performance, which in turn increases the risk of battery thermal runways and fire explosions. The potential failure rate becomes higher with interactions between the cells. For example, in a module of interconnected cells, during charging cycles, any degraded cell with a diminished capacity, upon reaching its full charge may continue to charge until the rest of the cells in the module reach their full charge. This overcharging of a single cell will overheat the battery, yielding to thermal runways.

In earlier work, [3], [4], the problem of aging propagation in interconnected systems for automotive batteries was formalized via a residual aging dynamics generator to monitor the degradation among cells. Cell-to-cell variations in Li-ion battery cells, not induced by aging but only by a statistical parameter variation, were analyzed in [5] as a critical factor in influencing the pack performance. In [6], preliminary results show that cell-to-cell variation within a battery pack, caused by differences in aging characteristics, *propagates* among cells within the pack. In [6], it was shown that the principle of modularity in predicting aging of a system from its components is lost as aging *furtively travels* into the system and retroactivity is observed. Retroactivity, studied in synthetic biology, is a phenomenon that causes the characteristics of a component to change upon interconnection, [7], [8]. A concept similar to retroactivity, namely *retroaction law*, is used in [9] to prove that the stress (or aging) that an element undergoes depends on its environment and its own damage through the retroaction law. In the context of battery packs, the presence of retroactivity may obviate modularity, making it a challenge to accurately predict the battery pack RUL (Remaining Useful Life) solely through component dynamics.

In this work, we develop a framework to model aging propagation through retroactivity in a series of interconnected cells. An electrochemical model that incorporates degradation parameters, in the form of SEI layer growth and ohmic drop across electrolyte, is employed to describe the dynamics of the battery, as opposed to an equivalent circuit model in [3], [4], [6]. Additionally, a two-state thermal model is utilized to predict the internal core temperature. The term representing the source of heat in the thermal model takes into consideration the electrochemical and aging processes. The semi-empirical aging model, which is characterized in terms of capacity fade and power fade, is directly correlated to the physical properties in the cell. A singular perturbation approach is used to single out the battery dynamics and develop a reduced order model to understand the effect of retroactivity on the degradation in interconnected cells.

The paper is structured as follows: Section II describes the Li-ion battery cell model combining the electrochemical dynamics, based on Single Particle Model (SPM), a two-state thermal model, and an aging model. Section III discusses the problem of aging in interconnected systems and provides the motivation to study the phenomenon of "retroactivity". In addition, we discuss the singular perturbation approach towards exploiting the three-time scale behavior of cell dynamics to obtain a reduced order model. Section IV puts forth the simulation results validating the framework of aging propagation through interconnected cells. Section V concludes the findings of the study, and lists any future work that is to be carried out.

II. Battery Cell Model

In this work, a Li-ion cell is modeled by its coupled combination of electrochemical, thermal, and aging dynamics. The mathematical models representing these dynamics and their mutual interdependence are described in this section.

A. Electrochemical Dynamics

A SPM of the cell is used in this work. A SPM is a reduced order electrochemical model that approximates the electrode as a single spherical particle. The SPM is simplified by assuming uniform concentration gradient in the electrolyte phase, neglecting the diffusion dynamics therein. This results in two Partial Differential Equations (PDE) characterizing the

Anirudh Allam (corresponding author) and Simona Onori are with the Automotive Engineering Department, Clemson University, Greenville, 29607, USA, {aallam, sonori}@clemson.edu

conservation of mass in the solid phase, given by Fick's law

$$\frac{\partial c_{s,j}}{\partial t} = D_{s,j}\left[\frac{2}{r}\frac{\partial c_{s,j}}{\partial r} + \frac{\partial^2 c_{s,j}}{\partial r^2}\right] \tag{1}$$

with the Neumann boundary conditions at the center and the surface of the spherical particle as

$$\left.\frac{\partial c_{s,j}}{\partial r}\right|_{r=0} = 0; \quad \left.\frac{\partial c_{s,j}}{\partial r}\right|_{r=R_j} = \pm\frac{I_{batt}}{F \cdot a_{s,j} \cdot D_{s,j} \cdot A \cdot L_j}$$

where $j \in$ [p,n] represents the positive or negative electrode, $c_{s,j}$ is the lithium concentration in the solid phase of the respective electrode, $D_{s,j}$ is the diffusion coefficient, t is the temporal coordinate, r is the radial coordinate, R_j is the radius of the spherical particle, I_{batt} is the input current, F is the Faradays constant, $a_{s,j}$ is the specific interfacial surface area, A is the cross sectional area of the cell, and L_j is the thickness of the electrode. The above PDEs are solved by radially discretizing them into a system of Ordinary Differential Equations (ODEs) using the Finite Difference Method (FDM) [10].

The electrochemical battery parameters are considered to be dependent on the cell's core temperature, T_c. In the literature, the diffusion coefficient $(D_{s,j})$ and the reaction rate constant (k_j) have an Arrhenius dependence on temperature given by

$$\psi(T_c) = \psi_{ref} \cdot exp\left[\frac{E_{a,\psi}}{R_g}\left(\frac{1}{T_{c,ref}} - \frac{1}{T_c}\right)\right] \tag{2}$$

where ψ stands for $D_{s,j}$ and k_j, $E_{a,\psi}$ is the activation energy associated with the diffusion and reaction rate, respectively, R_g is the universal gas constant, $T_{c,ref}$ is the reference core temperature, and T_c is the cell's operating core temperature. In addition, the open circuit potential (U_j) is approximated as a function of the surface concentration of the spherical particle $(c_{s,j,surf})$ and the core temperature by Taylor's expansion [11]

$$U_j(c_{s,j,surf}, T_c) = U_j(c_{s,j,surf}, T_{c,ref}) + \frac{\partial U_j}{\partial T_c}(T_c - T_{c,ref}) \tag{3}$$

The electrochemical dynamics is coupled to the aging dynamics through the inclusion of a model describing the side reaction that leads to the growth of the Solid Electrolyte Interphase (SEI) layer on the negative electrode. The SEI layer is formed due to solvent reduction on the surface of the active material that consumes cyclable lithium ions in the process [12]. The rate at which the SEI layer grows is given by

$$\frac{dL_{SEI}}{dt} = -\frac{i_s \cdot M_{SEI}}{2 \cdot F \cdot \rho_{SEI}} \tag{4}$$

where i_s is the side reaction current density, M_{SEI} is the molar mass of the SEI layer, and ρ_{SEI} is the SEI layer density.

The equations for overpotential (η_j) at the negative and positive electrode, with the inclusion of the potential drop across the SEI layer, are written as [13]

$$\begin{aligned}\eta_n &= \phi_{s,n} - \phi_{e,n} - U_n - \frac{I_{batt} \cdot L_{SEI}}{a_{s,n} \cdot A \cdot L_n \cdot K_{SEI}} \\ \eta_p &= \phi_{s,p} - \phi_{e,p} - U_p\end{aligned} \tag{5}$$

where the last term in the overpotential equation of the negative electrode represents the potential drop due to the SEI layer, and will be referred to as $I_{batt} \cdot R_{SEI}$ henceforth (where $R_{SEI} = \frac{L_{SEI}}{a_{s,n} \cdot A \cdot L_n \cdot K_{SEI}}$). In the above equation, $\phi_{s,j}$ and $\phi_{e,j}$ are the solid phase potential and the electrolyte potential at the respective electrodes, L_{SEI} is the thickness of the SEI layer, and K_{SEI} is the ionic conductivity in the SEI layer. The equation for the terminal voltage of the battery is then given by

$$\begin{aligned}V &= \phi_{s,p} - \phi_{s,n} \\ &= \eta_p - \eta_n + U_p - U_n + \phi_{e,p} - \phi_{e,n} - I_{batt} \cdot R_{SEI}\end{aligned} \tag{6}$$

where the term $\phi_{e,p} - \phi_{e,n}$ represents the potential drop across the electrolyte and can be represented as $I_{batt} \cdot R_e$, where R_e is referred to as the electrolyte resistance. The electrolyte resistance increases with aging, due to (a) reduced ionic conductivity in the electrolyte phase, and (b) increased SEI layer growth resulting in reduced porosity in the electrolyte phase of the negative electrode [13]. The rise in the electrolyte resistance over aging is assumed to be the primary reason for the rise in internal impedance of the cell.

The resulting equation for the terminal voltage of the battery is rewritten as

$$\begin{aligned}V \quad &= \eta_p(c_{s,p,surf}, T_c) - \eta_n(c_{s,n,surf}, T_c) + \\ &U_p(c_{s,p,surf}, T_c) - U_n(c_{s,n,surf}, T_c) - \\ &I_{batt}R_e - I_{batt}R_{SEI}\end{aligned} \tag{7}$$

The bulk concentration for the radially discretized electrode is computed using the volume averaging technique

$$c_{s,j,bulk} = \frac{1}{\frac{4}{3}\pi N^3}\sum_{k=1}^{N} 4\pi k^2 c_{s,j,k} \tag{8}$$

where N is the number of grid points obtained through FDM. The bulk concentration is normalized to obtain the bulk SOC, SOC_{bulk}, which varies between the two stoichiometric values $\theta_{j,100\%}$ and $\theta_{j,0\%}$, corresponding to the fully charged and discharged conditions for each electrode, through the relation [10]

$$SOC_{bulk} = \frac{c_{s,j,bulk}/c_{s,j,max} - \theta_{j,0\%}}{|\theta_{j,100\%} - \theta_{j,0\%}|} \tag{9}$$

Taking the derivative of (8) (and (9)) with respect to time, we obtain

$$\frac{dSOC_{bulk}}{dt} = \frac{3\sum_{k=1}^{N} k^2 \frac{dc_{s,j,i}}{dt}}{N^3 \cdot |\theta_{j,100\%} - \theta_{j,0\%}| \cdot c_{s,j,max}} \tag{10}$$

The capacity of the cell, Q (measured in Ah), in terms of electrochemical parameters is given by [10]

$$Q = F \cdot A \cdot L_j \cdot \epsilon_j \cdot c_{s,j,max} \cdot (\theta_{j,100\%} - \theta_{j,0\%})/3600 \tag{11}$$

where ϵ_j is the active material volume fraction of the electrode. Now, substituting (11) into the SOC dynamics (10), we have

$$\frac{dSOC_{bulk}}{dt} = \frac{3 \cdot F \cdot A \cdot L_j \cdot \epsilon_j}{3600 \cdot Q \cdot N^3}\sum_{k=1}^{N} k^2 \frac{dc_{s,j,i}}{dt} \tag{12}$$

B. Thermal Dynamics

A two-state lumped thermal model that describes the dynamics of the surface temperature and the core temperature of the cell is used. The underlying assumption is that the surface temperature is uniform throughout the surface and the internal temperature is uniformly distributed across the core. The mathematical representation of the two-state thermal model is given by [14]

$$\begin{cases} C_c \dfrac{dT_c}{dt} &= q_{cell} + \dfrac{T_s - T_c}{R_c} \\ C_s \dfrac{dT_s}{dt} &= \dfrac{T_{amb} - T_s}{R_u} - \dfrac{T_s - T_c}{R_c} \end{cases} \tag{13}$$

where T_s is the surface temperature, T_{amb} is the ambient temperature, C_c is the heat capacity of the core, C_s is the heat capacity of the surface, R_c is the conduction resistance between the surface and core, R_u is the convective resistance used to model the heat exchange with the environment, and q_{cell} is the irreversible heat generated due to the electrochemical reaction given as

$$q_{cell} = I_{batt} \cdot \Big(\eta_n(c_{s,n,surf}, T_c) - \eta_p(c_{s,p,surf}, T_c) + I_{batt} \cdot R_{SEI} + I_{batt} \cdot R_e \Big) \tag{14}$$

C. Aging Dynamics

We use a semi-empirical model to capture the dynamics of capacity loss and resistance increase in a cell. The model is identified as a function of the extracted ampere hours (Ah), obtained as $Ah = \int \frac{|I_{batt}|}{3600}$, and severity factors (viz. SOC_{bulk}, C-rate (I_c), core temperature (T_c)). The loss in capacity (Q_{loss}) and increase in resistance $(R_{e,inc})$ are defined as follows [6]:

$$Q_{loss} = \frac{Q_0 - Q}{Q_0} \cdot 100; \quad R_{e,inc} = \frac{R_e - R_{e,0}}{R_{e,0}} \cdot 100 \tag{15}$$

where Q is the cell capacity subject to aging and Q_0 is the capacity at Beginning of Life (BOL), R_e is the electrolyte resistance and $R_{e,0}$ is its value at BOL.

The semi-empirical model identified for capacity loss and resistance increase are nonlinear functions of the severity factors $[SOC_{bulk}, I_c, T_c,]$, and $[I_c, T_c]$ respectively, given by [15], [6]

$$\begin{cases} \sigma_{funct,Q}(SOC_{bulk}, I_c, T_c) &= (\alpha_Q \, SOC_{bulk} + \beta_Q) \cdot \\ & \quad e^{\left(\dfrac{-E_{a,Q} + \eta_Q I_c}{R_g(T_c + 273.15)} \right)} \cdot Ah^z \\ \sigma_{funct,R_e}(I_c, T_c) &= \left(\alpha_{R_e} + \mu_{R_e} \, e^{(\gamma_{R_e} \, I_c)} \right) \cdot \\ & \quad e^{\left(\dfrac{-E_{a,R_e}}{R_g(T_c + 273.15)} \right)} \cdot Ah \end{cases} \tag{16}$$

where $E_{a,Q}, E_{a,R_e}$ are the activation energy corresponding to capacity loss and resistance increase respectively, while $\alpha_Q, \beta_Q, \eta_Q, z, \alpha_{R_e}, \mu_{R_e}$, and γ_{R_e} are parameters obtained by fitting the model to the experimental data [16].

The capacity and resistance dynamics of the cell with respect to time are given as follows [6]

$$\begin{cases} \frac{dQ}{dt} &= -\frac{Q_0}{100} \, \sigma_{funct,Q}(SOC_{bulk}, I_c, T_c) \; z \; Ah^{z-1} \frac{|I_{batt}|}{3600} \\ \frac{dR_e}{dt} &= \frac{R_{e,0}}{100} \, \sigma_{funct,R}(I_c, T_c) \cdot \frac{|I_{batt}|}{3600} \end{cases} \tag{17}$$

In this paper, we assume that capacity loss is primarily due to loss of cyclable lithium ions, that are lost to the side reactions resulting in the growth of the SEI layer. This can be written as [13]

$$\frac{dQ}{dt} = i_s \cdot a_{s,n} \cdot A \cdot L_n \tag{18}$$

From (4) and (18), the rate of capacity loss is related to the rate of SEI layer growth as follows:

$$\frac{dQ}{dt} = -\frac{dL_{SEI}}{dt} \cdot \frac{2 \cdot F \cdot \rho_{SEI} \cdot a_{s,n} \cdot A \cdot L_n}{M_{SEI}} \tag{19}$$

III. Aging in Interconnected Systems

Battery modules for automotive applications are large scale systems consisting of several interconnected cells in a series and/or parallel configuration. Due to manufacturing variances and/or existence of temperature gradient within modules, over a period of prolonged use, each cell ages at a different rate causing dissimilar aging within interconnected cells. The dissimilar aging of cells may further accentuate the temperature differences between a cell and its neighboring cells.

Let us consider a module of four fresh cells $i-1$, i, $i+1$, and $i+2$ connected in series. The thermal dynamics of every cell in the module is altered to accommodate the thermal interaction occurring between its neighboring cells. The surface thermal dynamics of a cell i connected to cells $i-1$ and $i+1$ is given by

$$C_{s,i} \frac{dT_{s,i}}{dt} = \frac{T_{amb} - T_{s,i}}{R_{u,i}} - \frac{T_{s,i} - T_{c,i}}{R_{c,i}} - \frac{T_{s,i} - T_{s,i-1}}{R_{p,i-1}} - \frac{T_{s,i} - T_{s,i+1}}{R_{p,i+1}} \tag{20}$$

In the above equation, the surface thermal dynamics of cell i is modified with the inclusion of two terms that represent heat exchange between the neighboring cells. The conduction resistances within the battery pack $R_{p,i-1}$ and $R_{p,i+1}$ model the heat exchange between the cell i and the upstream cell $i-1$, and cell i and the downstream cell $i+1$, respectively. The core temperature of cell i varies according to the surface-core relation expressed in (13). Rearranging (20) yields the following equation

$$\frac{dT_{s,i}}{dt} = \frac{T_{amb}}{R_{u,i} C_{s,i}} + \frac{T_{c,i}}{R_{c,i} C_{s,i}} - T_{s,i} R_{comb,i} + \boxed{\frac{T_{s,i-1}}{R_{p,i-1} C_{s,i}}} + \boxed{\frac{T_{s,i+1}}{R_{p,i+1} C_{s,i}}} \tag{21}$$

where R_{comb} is the lumped resistance given by $\left(\frac{1}{R_u} + \frac{1}{R_{c,i}} + \frac{1}{R_{p,i-1}} + \frac{1}{R_{p,i+1}} \right)$. The two boxed terms, represent the heat transfer from the upstream cell $i-1$ and

the downstream cell $i+1$. These two terms are responsible to alter the thermal dynamics of cell i.

The existence of the boxed terms in (21) is demonstrated through experiments conducted on a module of four fresh cells connected in series, as shown in Figure 1. The cathode chemistry is Lithium Nickel Manganese Cobalt Oxide (NMC) and each cell has a rated capacity of $2.1Ah$. The ambient temperature is set to $20\,^{\circ}\mathrm{C}$ and the distance between each cell in the module is approximately $1-1.3cm$.

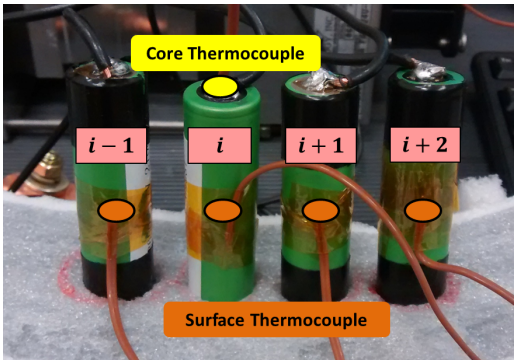

Fig. 1: Setup of four Li-ion NMC 18650 cells connected in series with four thermocouples to measure the surface temperature of each cell and one thermocouple to measure the core temperature of cell i.

We subject cell i to the current profile in Figure 2(a) in both, an isolated and interconnected (as in Figure 1) configuration. A difference in the core and surface temperature of cell i is observed, as plotted in Figure 2(b). This difference in temperature is the display of the loss of thermal modularity; wherein modularity is defined as the property of predicting the behavior of a large scale system based on the input/output behavior of its composing units [7]. Such a loss of modularity may be more pronounced in larger battery modules, where numerous strings of cells in series and parallel are placed very close to each other, and each cell is thermally interlinked to many of its neighboring cells. Through this, we understand that the behavior of a single cell changes upon interconnection, making it a challenge to accurately predict the thermal behavior of a battery module by looking at the thermal dynamics of a single cell in the module.

In [6], the authors adopted the phenomenon of retroactivity, originally proposed for transcriptional modules [7], to the context of interconnected battery cells[1]. Retroactivity manifests itself through thermal interconnections between cells (boxed terms in (21)). In light of retroactivity, within the context of assessment of State-of-Health (SOH) and aging of the battery pack, it is postulated that the degradation of an upstream cell i, is affected, indistinctly, by the degradation of the downstream cell $i+1$, through retroactivity. Degradation in cell $i+1$, for example, in terms of resistance increase $(R_{e,i+1}+\Delta R_{e,i+1})$, causes an increase in its core temperature $(T_{c,i+1}+\Delta T_{C,i+1})$ due to higher Joule heating that affects the thermal dynamics of the upstream cell i (through

[1]Retroactivity, in our context, is defined as the phenomenon in which the dynamics of a cell are altered due to an upstream and a downstream cell.

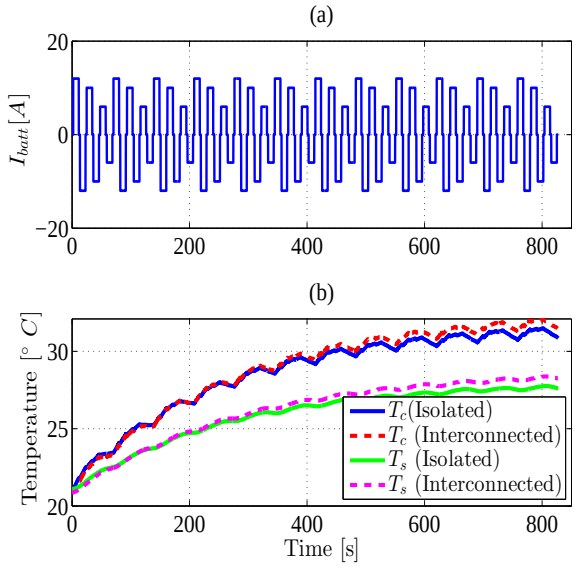

Fig. 2: (a) Current profile with ample excitation subjected to the series configuration. (b) Comparison of core and surface temperature of cell i when it is isolated and when it is interconnected to other cells.

retroactivity) making it operate at a higher core temperature $(T_{c,i}+\Delta T_{C,i})$, ultimately resulting in cell i's accelerated degradation $(R_i+\Delta R_i)$.

Remark: From the knowledge of the cell dynamics, we understand that the thermal dynamics is fast, SOC_{bulk} dynamics is semi-slow, and aging dynamics is slow [6]. In order to quantify the effect of retroactivity on the slow aging dynamics, we look to exploit this three time-scale behavior of the cell. We introduce a "slow" time scale τ, and normalize the cell dynamics given in (12), (13), and (17) with respect to the slow dynamics, i.e. aging, to obtain a set of equations as given below

$$\begin{cases} \dfrac{dQ}{d\tau} & = -Q_0\cdot(\alpha_Q\, SOC_{bulk}+\beta_Q)\cdot \\ & \quad z\cdot\ Ah^{z-1}\cdot|I_{batt}|\cdot \\ & \quad e^{\left(\dfrac{-E_a+\eta_Q I_c}{R_{gas}(T_c+273.15)}\right)} \\ \dfrac{dR_e}{d\tau} & = R_{e,0}\cdot\left(\alpha_{R_e}+\mu_{R_e}\ e^{(\gamma_{R_e}\ I_c)}\right)\cdot|I_{batt}|\cdot \\ & \quad e^{\left(\dfrac{-E_{a,R_e}}{R_{gas}(T_c+273.15)}\right)} \\ \epsilon_1\cdot\dfrac{dSOC_{bulk}}{d\tau} & = \dfrac{AL_j\epsilon_j}{QN^3}\sum_{i=1}^{N} i^2\dfrac{dc_{s,j,i}}{d\tau} \\ \epsilon_1\cdot\epsilon_2\cdot\dfrac{dT_c}{d\tau} & = \dfrac{q_{cell}}{C_c}+\dfrac{T_s-T_c}{R_c\cdot C_c} \\ \epsilon_1\cdot\epsilon_2\cdot\dfrac{dT_s}{d\tau} & = \dfrac{T_{amb}-T_s}{R_u\cdot C_s}-\dfrac{T_s-T_c}{R_c\cdot C_s} \end{cases} \tag{22}$$

where $\epsilon_1=1/100$, $\epsilon_2=1/3600$, and $\tau=\epsilon_1\cdot\epsilon_2\cdot t$. The choice of ϵ_1 and ϵ_2 is made by identifying constants that are multiplied to the highest derivative of the states in the equations of the cell dynamics. We notice that the above set of state variables represent a three-time scale system in the

standard singularly perturbed form [17]:

$$\begin{cases} \dot{x} & = f(x,y,z,u) & \rightarrow Slow \\ \epsilon_1 \cdot \dot{y} & = g(x,y,z,u) & \rightarrow Semi-slow \\ \epsilon_1 \cdot \epsilon_2 \cdot \dot{z} & = h(x,y,z,u) & \rightarrow Fast \end{cases} \tag{23}$$

where x, y, z are the set of slow, semi-slow, and fast variables respectively, and ϵ_1, ϵ_2 are the perturbation parameters such that $0 < \epsilon_1 \cdot \epsilon_2 \ll \epsilon_1 \ll 1$ and hence $\epsilon_2 \ll 1$. The general evolution scheme of a three-time scale system involves a boundary-layer system and a slow manifold. The initial interval where the fast variable, starting from an initial value, undergoes a rapid transient to reach its quasi steady state, is described by the boundary-layer system. The semi-slow and slow variables evolve on a slow manifold, by setting $\epsilon_1 \cdot \epsilon_2$ to 0 in the fast variable, such that any trajectory on this manifold will remain in the manifold for all future time [18].

Observation: In system (22), the fast thermal variables, $T = [T_c, T_s]$, converge to their steady-state values, $\bar{T} = [\bar{T}_c, \bar{T}_s]$, thanks to the asymptotic stability of the boundary-layer system. One can see this by performing a change of variables that shifts the equilibrium of the boundary-layer to the origin by introducing the error dynamics $\hat{T} = T - \bar{T}$. By setting $\epsilon_1 \cdot \epsilon_2 = 0$, we have

$$\begin{cases} \bar{T}_c & = q_{cell} R_c + \bar{T}_s \\ \bar{T}_s & = \dfrac{R_u R_c}{R_u + R_c} \left(\dfrac{T_{amb}}{R_u} + \dfrac{\bar{T}_c}{R_c} \right) \end{cases} \tag{24}$$

To obtain the boundary-layer system, we revert back to the fast time scale t, where the semi-slow and slow variables freeze in their respective initial states. Substituting $T = \hat{T} + \bar{T}$ in the thermal dynamics given in (22), we obtain the boundary-layer system

$$\begin{cases} \dfrac{d\hat{T}_c}{dt} & = \dfrac{-1}{R_c C_c} \hat{T}_c + \dfrac{1}{R_c C_c} \hat{T}_s \\ \dfrac{d\hat{T}_s}{dt} & = \dfrac{1}{R_c C_s} \hat{T}_c - \dfrac{(R_u + R_c)}{R_c R_u} \hat{T}_s \end{cases} \tag{25}$$

where R_c, C_c, R_u, C_s are non-negative constants. The origin of the boundary-layer system is globally exponentially stable, if the condition $\frac{(R_u + R_c)}{R_u} > \frac{1}{C_s}$ is satisfied. We conclude that $T = \bar{T} + \mathcal{O}(\epsilon_1 \cdot \epsilon_2)$ exists for time $t \in [t_1, t_2]$ [18]. For all $t \in [t_0, t_2]$, where $t_0 < t_1 < t_2$, we can comment that the motion of the semi-slow and slow variables on the slow manifold will be always confined in a bounded space defined by their respective upper and lower limits, such that $SOC_{bulk} \in [SOC_{bulk,min}, SOC_{bulk,max}]$, $Q_{loss} \in [Q_{loss,min}, Q_{loss,max}]$, and $R_{e,inc} \in [R_{e,inc,min}, R_{e,inc,max}]$, where the minimum and maximum limits are determined by the specific application or the physical constraints of the cell[2]. By substituting the quasi-steady state of thermal dynamics($\bar{T}_c = q_{cell}(R_u + R_c) + T_{amb}$), we arrive at the reduced order slow model, for both capacity and resistance, as follows

$$\begin{cases} \dfrac{dQ}{d\tau} & = -Q_0(\alpha_Q \, SOC_{bulk} + \beta_Q) \cdot \; z \; Ah^{z-1} \cdot |I_{batt}| \\ & \quad e^{\left(\dfrac{-E_a + \eta_Q I_c}{R_{gas}((q_{cell}(R_u + R_c) + T_{amb} + 273.15)} \right)} \\ \dfrac{dR_e}{d\tau} & = R_{e,0} \left[\alpha_{R_e} + \mu_{R_e} \, e^{(\gamma_{R_e} \; I_c)} \right] \cdot |I_{batt}| \\ & \quad e^{\left(\dfrac{-E_{a,R_e}}{R_{gas}((q_{cell}(R_u + R_c) + T_{amb} + 273.15)} \right)} \end{cases} \tag{26}$$

The above reduced order model for an isolated cell is extended to interconnected cells to study aging propagation through retroactivity with the inclusion of the altered thermal dynamics due to interconnection. The slow manifold and the simulated trajectory of the dynamics of an isolated cell are shown in Figure 3.

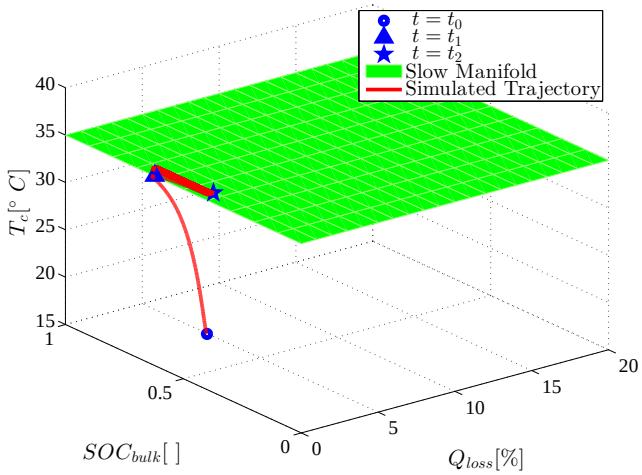

Fig. 3: Simulation of three-time scale evolution of cell dynamics. The initial point at the start of the simulation is at time $t = t_0$, where $T_c = 20\,^\circ$C, $T_{amb} = 35\,^\circ$C, $SOC_{bulk} = 0.4$, and $Q_{loss} = 0\%$. Input to the simulation is a charge-discharge cycle of $1C$ for a period of one day. At time $t = t_1$, the initial (boundary-layer) interval ends with T_c converging into the slow manifold. The motion of SOC_{bulk} and Q_{loss} on the slow manifold is bounded by the limits, specific to the application, given by $SOC_{bulk} \in [0.3, 0.8]$, and $Q_{loss} \in [0, 20]\%$, until the end of simulation time given by $t = t_2$.

IV. Simulation Results

The proposed framework of aging propagation in interconnected cells through retroactivity is validated through simulation results. Two scenarios are simulated and compared to gauge the effect of retroactivity in a module of four cells in series, where each cell is referred to by its position. The first scenario assumes the absence of retroactivity in the module, whereas the second scenario assumes the presence of retroactivity acting on the cells through their respective thermal interconnections. In both scenarios, the cell in position # 2 is aged, with its aging variables initialized as $Q_{loss} = 5\%, R_{e,inc} = 2\%$ [19], while the remaining cells in the module are fresh. The input to both scenarios is a charge-discharge cycle of $2C$ spanning the range of SOC from 40 to 70%, for a period of 45 days. The ambient temperature

[2] Q_{loss} and $R_{e,inc}$ are related to Q and R_e through (15).

is set to $45\,^{\circ}\mathrm{C}$ and the initial core temperature of each cell is $20\,^{\circ}\mathrm{C}$. The difference (ΔX_i) in the core temperature, SEI layer thickness, and the electrolyte resistance of each cell, between the two scenarios, is obtained using

$$\Delta X_i = X_{i,r} - X_{i,nr} \tag{27}$$

where i refers to the cell position, $X \in [T_c, L_{SEI}, R_e]$, and subscripts r and nr represent the second and first scenario respectively. A positive value of ΔX_i indicates the adverse effect of the presence of retroactivity on each cell in the module, as plotted in Figure 4, wherein the degradation in the cell in position # 2 has propagated to its neighboring fresh cells.

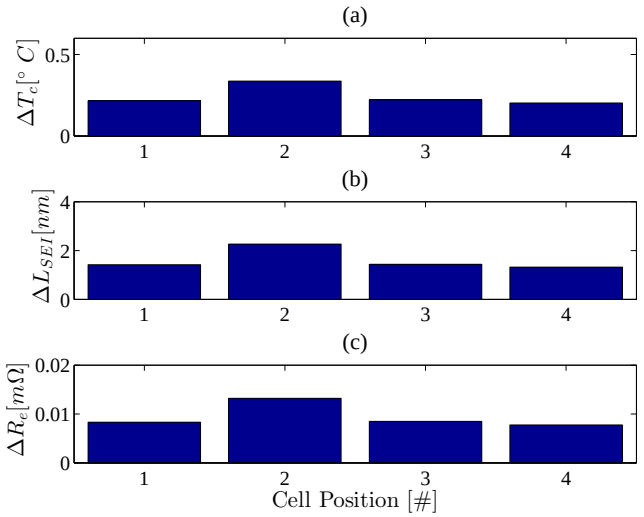

Fig. 4: Effect of retroactivity on four cells connected in series in terms of increase in (a) Core temperature, (b) SEI layer thickness, and (c) Electrolyte resistance

This propagation of aging through retroactivity can be minimized by properly designing thermal management units in way to enforce the modules/pack to retain the isolated behavior of their constituting cells, i.e. minimizing temperature gradient. This can be achieved, for instance, using phase change material [20] to passively control and reduce thermal gradient and prevent the propagation effects.

V. Conclusion and Future Work

We presented a framework exhibiting the propagation of aging through thermal interconnections between connected cells using an electrochemical degradation battery model, two-state thermal model, and an aging model. The three-time scale behavior of cell dynamics is exploited using the singular perturbation theory to obtain a slow reduced order model. The simulated trajectory exhibiting the three-time scale behavior of the cell dynamics is displayed. Simulation results showing aging propagation, due to retroactivity, are presented in terms of increase in the SEI layer thickness and electrolyte resistance of each cell in the module. Going forward, the reduced order model for interconnected cells will be used to quantify retroactivity in terms of increase in SEI layer thickness and electrolyte resistance.

References

[1] R. Parrish, K. Elankumaran, M. Gandhi, B. Nance, P. Meehan, D. Milburn, S. Siddiqui, and A. Brenz, "Voltec battery design and manufacturing." SAE International, 2011.

[2] E. Musk, "Model S fire," 2014.

[3] S. Onori, G. Rizzoni, and A. Cordoba-Arenas, "A prognostic methodology for interconnected systems: preliminary results," in *8th IFAC International Symposium on Fault Detection, Supervision and Safety of Technical Processes, Mexico DF, Mexico*, 2012.

[4] A. Cordoba-Arenas, S. Onori, G. Rizzoni, and G. Fan, "Aging propagation in interconnected systems with an application to advanced automotive battery packs." 7th IFAC Symposium on Advances in Automotive Control, Tokyo, Japan, Sept. 4-7, 2013, pp. 703–716.

[5] A. Cordoba-Arenas, S. Onori, and G. Rizzoni, "A control-oriented lithium-ion battery pack model for plug-in hybrid electric vehicle cycle-life studies and system design with consideration of health management," *JOURNAL OF POWER SOURCES*, vol. 279, pp. 791–808, 2015.

[6] A. Allam, S. Onori, S. Marelli, and C. Taborelli, "Battery health management system for automotive applications: A retroactivity-based aging propagation study." Proceedings of the American Control Conference, 2015, pp. 703–716.

[7] D. D. Vecchio, A. J. Ninja, and E. D. Sontag, "A System Theory with Retroactivity: Application to Transcriptional Modules," *Proceedings of the American Control Conference*, pp. 1368–1373, 2008.

[8] S. Jayanthi and D. Del Vecchio, "Retroactivity attenuation in bio-molecular systems based on timescale separation," *IEEE Transactions on Automatic Control*, vol. 56, no. 4, pp. 748–761, 2011.

[9] G. Vinson, P. Ribot, and M. Combacau, "A generic ageing model for prognosis - application to permanent magnet synchronous machines," vol. 5, no. 12. Second European Conference of the Prognostics and Health Management Society, 2014, p. 703716.

[10] D. Di Domenico, A. Stefanopoulou, and G. Fiengo, "Lithium-ion battery state of charge and critical surface charge estimation using an electrochemical model-based extended kalman filter," *Journal of Dynamic Systems, Measurement, and Control*, vol. 132, no. 6, p. 61302, 2010.

[11] M. Guo, G. Sikha, and R. E. White, "Single-particle model for a lithium-ion cell: Thermal behavior," *Journal of The Electrochemical Society*, vol. 158, no. 2, p. A122, 2011.

[12] M. Pinson and M. Bazant, "Theory of sei formation in rechargeable batteries: Capacity fade, accelerated aging and lifetime prediction," *Journal Of The Electrochemical Society*, vol. 160, no. 2, pp. A243–A250, 2013;2012;.

[13] E. Prada, D. Di Domenico, Y. Creff, J. Bernard, V. Sauvant-Moynot, and F. Huet, "A simplified electrochemical and thermal aging model of lifepo4-graphite li-ion batteries: Power and capacity fade simulations," *JOURNAL OF THE ELECTROCHEMICAL SOCIETY*, vol. 160, no. 4, pp. A616–A628, 2013.

[14] X. Lin, H. E. Perez, S. Mohan, J. B. Siegel, A. G. Stefanopoulou, Y. Ding, and M. P. Castanier, "A lumped-parameter electro-thermal model for cylindrical batteries," *Journal of Power Sources*, vol. 257, pp. 1–11, 2014.

[15] A. Cordoba-Arenas, S. Onori, Y. Guezennec, and G. Rizzoni, "Capacity and power fade cycle-life model for plug-in hybrid electric vehicle lithium-ion battery cells containing blended spinel and layered-oxide positive electrodes," *Journal of Power Sources*, vol. 278, pp. 473–483, 2015.

[16] G. Suri and S. Onori, "A control-oriented cycle-life model for hybrid electric vehicle lithium-ion batteries," *Energy*, vol. 96, pp. 644–653, 2016.

[17] S. Esteban, F. Gordillo, and J. Aracil, "Three-time scale singular perturbation control and stability analysis for an autonomous helicopter on a platform," *International Journal of Robust and Nonlinear Control*, vol. 23, no. 12, pp. 1360–1392, 2013.

[18] H. K. Khalil, *Nonlinear systems*, 3rd ed. Upper Saddle River, N.J: Prentice Hall, 2002.

[19] P. Spagnol, S. Onori, N. Madella, Y. Guezennec, and J. Neal, "Aging and characterization of Li-ion batteries in a hev application for lifetime estimation," *6th IFAC Symposium Advances on Automotive Control, Munich Germany*, July 12-14 2010.

[20] P. Goli, S. Legedza, A. Dhar, R. Salgado, J. Renteria, and A. Balandin, "Graphene-enhanced hybrid phase change materials for thermal management of li-ion batteries," *JOURNAL OF POWER SOURCES*, vol. 248, pp. 37–43, 2014.